Numerical analysis of the distribution of combustion products from methane explosions in a full-scale tunnel using all-speed CFD code GASFLOW-MPI

Yuntao Liang, Baiwei Lei, Shuanglin Song, Jianjun Xiao, Mike Kuznetsov & Thomas Jordan

Numerical analysis of the distribution of combustion products from methane explosions in a full-scale tunnel using all-speed CFD code GASFLOW-MPI

Yuntao Liang[a], Baiwei Lei[a,b], Shuanglin Song[a], Jianjun Xiao[c], Mike Kuznetsov[c], and Thomas Jordan[c]

[a]State Key Laboratory of Coal Mine Safety Technology, Shenyang, China; [b]School of Emergency Management and Safety Engineering, China University of Mining & Technology (Beijing), Beijing, China; [c]Institute of Thermal Technologies and Safety, Karlsruhe Institute of Technology, Eggenstein-Leopoldshafen, Germany

ABSTRACT

Methane explosions are among the main hazards in coal mines. Shock waves from methane explosions can cause damage near the explosion site, and combustion products can spread along the tunnel to locations far from the explosion source and endanger the lives and health of personnel. Therefore, the study of the propagation patterns of methane explosion shock waves and the distribution of high-temperature combustion products in tunnels. has significance for emergency decision-making in the event of methane explosions in a mine. This study uses the 3D Computational Fluid Dynamics (CFD) program GASFLOW-MPI, which models the one-step methane combustion mechanism with the addition of a heat transfer model. The methane explosion process is simulated and reproduced at the Lake Lynn Experimental Mine (LLEM) to analyze the process of gas deflagration. The results reveal that the overpressure in the tunnel after the methane explosion oscillates and decays with time. Gaseous products of the explosion "expand and compress" and flow back and forth in accordance with the oscillation of overpressure. The maximum expansion ratio of the CO_2 concentration isosurfaces of 0.5% in the heat transfer simulation is 6.21, whereas the volume expansion ratio is 3.78 once the flow field stabilizes. The distribution of combustion products along the alleyway exhibits a Gaussian decay trend. The range of gaseous product distribution and temperature fields in the adiabatic tunnel is significantly higher than that in the heat transfer simulations, thus indicating that heat loss significantly influences the temperature characteristics and distribution pattern of combustion products in the full-scale tunnel.

Introduction

Methane explosions, which generate shock waves and harmful gases at high temperatures, are among the worst coal mine disasters. The destructive effect of the gas explosion shock wave is very strong, which will cause damage to people and ventilation facilities near the explosion site. The high-temperature gaseous products produced by the gas explosion spread with the wind flow, thus endangering the lives of mine workers. Combustible gas explosions can be divided into deflagration and detonation forms based on the difference in combustion reaction speed (Thomas 2012). Researchers have found that shock waves propagate at supersonic speeds during combustible gas detonations (Cheng et al. 2021), which are more destructive (Xiao and Oran 2020; Zipf et al.

CONTACT Baiwei Lei leibws@163.com School of Emergency Management and Safety Engineering, China University of Mining & Technology, Beijing 100083, China

2014). Turbulence induced by narrow channels, obstacles, and other factors can accelerate the transition from deflagration to detonation in gas explosions (Huang, Gao, and Wang 2018; Kuznetsov et al. 2002; Valiev et al. 2010). However, current experimental and numerical simulation studies on coal mine methane explosions indicate that the variation patterns of shock wave overpressure, velocity, and other characteristics observed in the roadway are consistent with the phenomenon of methane deflagration (Gao et al. 2020; Pang et al. 2012; Wang, Zhao, and Addai 2017; Zhang and Ma 2015; Zhu et al. 2020). Therefore, researchers have performed numerous numerical simulations and experimental studies on the factors affecting methane explosions in spherical devices and pipelines (Vishwakarma, Ranjan, and Kumar 2014). The effects of various volume sizes and gas concentrations on maximum methane explosion pressure and flame propagation velocity in a confined space have been studied (Cammarota et al. 2010; Dahoe and De Goey 2003; Gieras and Klemens 2009; Kuznetsov et al. 2022; Mittal 2017). Owing to the high cost of methane explosion experiments in real mines and the lack of actual measured data, methane explosion experiments typically performed in pipelines or numerical simulations are used to analyze the characteristics of methane explosions. Further, some researchers have investigated the impact of parameters, such as pipe bifurcation, bending, obstacles, and cross-sectional area, on flame acceleration and shock wave propagation (Ajrash, Zanganeh, and Moghtaderi 2017, 2018; Kundu, Zanganeh, and Moghtaderi 2016; Kuznetsov et al. 2022; Li et al. 2021; Zhu et al. 2021).

Considering the scale effect involved in the process of methane explosion (Tan et al. 2021), small-scale methane explosion experiments can obtain only a qualitative trend of explosion parameters. The United States Bureau of Mines (USBM) (Cashdollar, Urosek, and Sapko 2009) conducted numerous methane explosion experiments under full-scale conditions to analyze the attenuation pattern of the methane explosion shock wave and the damage caused by the shock wave to the containment wall. The Chongqing Institute of Coal Science in China conducted an experimental study on the attenuation pattern of methane explosion shock waves in full-scale experimental tunnels (Qu, Zhou, and Wang 2008). Several researchers have conducted numerical simulation studies based on methane explosions in full-scale tunnels (Zipf et al. 2007) and verified the accuracy of FLACS and AUTOREGAS in modeling and analyzing the propagation pattern of methane explosion shock waves based on a methane explosion experiment in LLEM in the United States (Davis, Engel, and Van Wingerden 2014) using FLACS to analyze the propagation of shock waves in the Upper Big Branch (UBB) explosion accidents. Zipf et al. (2007) investigated the effect of confined walls on blocking gas excitations using FLACS and AUTOREGAS. Zhu et al. (2020) used FLACS to analyze the impact of tunnel structure on methane explosion characteristics and the impact of gas concentration and other parameters on the propagation of methane explosion shock waves at various scales. The aforementioned numerical simulation studies only examined shockwave propagation following a methane explosion, and the majority of them were simulated under adiabatic conditions. Goldfarb et al. (1999 reported that thermal radiation significantly affects the explosion of combustible gases. Ye et al. (2017) demonstrated that heat transfer significantly affects the methane explosion's intensity and flame propagation speed. Luo and Cheng (2013) analyzed the effect of heat loss on the peak methane explosion pressure using FLACS simulations.

However, their study lacked an analysis of the effect of heat loss on the distribution patterns of the combustion products (Lv, Liu, and Wang 2013). Assuming that the high-temperature gas accumulates in the tunnel and used Fluent simulations to analyze the heat transfer process between the high-temperature gas and the wall. However, methane explosions cause the transport of combustion products, and the distribution of gas concentration in the tunnel is uneven. Therefore, predicting the distribution and heat-transfer dynamics of combustion products is challenging.

Numerical simulations can provide details on the shock wave and flow of combustion products after a methane explosion. Given the significant differences in time scales of shock wave propagation and combustion product flow, a method appropriate for all-speed is required to study the variation in the characteristic parameters during the entire process of a methane explosion. This can address the issue of the high computational time and cost of a methane explosion. Such a method must

simultaneously calculate the methane explosion shock wave and the migration law of combustion products.

In summary, numerous studies have focused on the attenuation pattern of shock waves generated by methane explosions; however, studies on the distribution of combustion products arising from methane explosions are limited. Due to the shockwave propagation time is much shorter than that of high-temperature hazardous gases, the toxic and harmful gases generated by methane explosions pose a severe threat to the safety of mine workers. Studying the diffusion and distribution patterns of combustion products from methane explosions in mine tunnels is crucial to improving the emergency response for mine rescue operations. Therefore, this study used GASFLOW-MPI, which supports all-speed simulation calculations, to simulate methane explosions. Focusing on the pressure, velocity, and temperature fields, the temperature characteristics, and distribution pattern of methane explosion gaseous products in a full-scale tunnel were analyzed in adiabatic and heat transfer simulations, thereby providing a theoretical basis for formulating measures to prevent and control methane explosion accidents in mining.

Numerical methods

GASFLOW-MPI is an all-speed CFD program with parallel scalability that solves compressible Navier – Stokes equations based on the all-speed arbitrary Lagrangian – Eulerian method. This has been validated in the simulation of combustible gas transport diffusion, combustion, and explosion (Xiao et al. 2017).

Assumption

The explosion process of flammable gases in a confined space is very complex. To simplify the mathematical model and enable fast calculation, the following assumptions are made:

(a) The tunnel walls are assumed to be smooth during the explosion process.
(b) Assuming no obstacles other than sealing wall within the roadway.
(c) The initial combustible premixed gas and combustion products are assumed to follow the ideal gas equation.
(d) The methane explosion is assumed to be an irreversible one-step reaction.

Governing equations

Continuity equation is shown as Equation (1) (Travis and Koch 2014).

$$\frac{\partial}{\partial t}\int_V \Phi dV \quad \int_S \Phi(b \quad u)AdS + \int_V S_\Phi dV \tag{1}$$

Mass conservation equation is shown as Equation (2) (Travis and Koch 2014).

$$\frac{\partial}{\partial t}\int_V \rho dV \quad \int_S \rho(b \quad u)AdS + \int_V S_\rho dV \tag{2}$$

Momentum conservation equation is shown as Equation (3) (Travis and Koch 2014).

$$\frac{\partial}{\partial t}\int_V \rho \cdot \mathrm{u}dV \quad \int_S \rho \cdot \mathrm{u}(b \quad u)AdS + \int_S \mathrm{p}dS + \int_V \rho \cdot gdV \quad \int_S (V \cdot A)dS \quad \int_S (D_d A)dS + \int_V S_\mathrm{m} dV \tag{3}$$

Energy conservation equation is shown as Equation (4) (Travis and Koch 2014).

$$\frac{\partial}{\partial t}\int_V \rho \cdot I dV \quad \int_S \rho \cdot I(b \quad u) A dS \quad \int_S \mathrm{p}(\mathrm{u} \cdot \mathrm{A}) dS \quad \int_V \left[\frac{p}{V}\frac{\partial V_{H_2O}}{\partial t}\right] dV \quad \int_S (q \cdot A) dS \quad \int_V S_I dS \tag{4}$$

In the above equations, V and S denote the volume and surface area of the control body, respectively; $\rho$is the density of the fluid; I is the internal energy of the fluid; t is the viscous stress tensor of the fluid; D_d is the tension stress tensor of the fluid; q is the fluid energy flow vector; S_Φ, S_ρ, S_m, and S_I are the source terms.

Heat transfer model

A heat-transfer model was developed considering that the heat released from a methane explosion in a full-scale tunnel is lost in three ways, namely, convective (Siegel et al. 1992), radiation (Xiao, Kuznetsov, and Travis 2018), and conductive (Xiao, Travis, and Kuznetsov 2015) heat transfer between the wall surface and gaseous products from explosions. The validity of this heat transfer model was verified by (Lei et al. 2022, 2023).

The convective heat transfer model is shown as Eq.. 5 (Fernández-Tarrazo et al. 2006).

$$\int_S S_{I,convection} dV \quad \sum_S h_s A_s (T_s \quad T) \tag{5}$$

where h_s is the heat exchange coefficient between the gas mixture and solid wall, T_s is the temperature of the solid wall, T is the temperature of the gas mixture, A_s is the heat exchange area between the gas mixture and solid wall.

The gas thermal radiation transport model is shown as Eq.. 6 (Siegel and Howell 1992; Xiao, Kuznetsov, and Travis 2018).

$$\frac{1}{c}\frac{\partial E(\mathrm{r},\Omega,\mathrm{t})}{\partial t} + l_i \frac{\partial E(\mathrm{r},\Omega,\mathrm{t})}{\partial x_i} \quad \alpha E(\mathrm{r},\Omega,\mathrm{t}) + \frac{\alpha\sigma T^4}{\pi} \tag{6}$$

where c is the speed of light; $E(\mathrm{r},\Omega,\mathrm{t})$is the specific radiation intensity, which is a function of the position vector r, directional vector U, and time t; l_i is the direction cosine of vector U with respect to the coordinate directions x_i; $\alpha$is the absorption coefficient; σ is the Stefan – Boltzmann constant.

Simulation model parameters

Lake lynn experimental mine model

The LLEM is a full-scale coal mine that is used for fire and explosion experiments. This study adopted the methane explosion experiment number #501 in the LLEM. The geometric model is shown in Figure 1. In Figure 1, the black dots indicate sensor positions, character C indicates that the measuring point is located in aisle C, and numbers denote the sensor's distance, in m, from the head of the aisle. The experimental gas was collected at the head of the C aisle, with a gathering length of 15.6 m, as shown in the orange area of Figure 1. The mixture consisting of 187.2 m^3 of 10% methane and 90% air was sealed using a plastic film and ignited. Details on the LLEM and #501 methane explosion experiments can be found in (Cashdollar, Urosek, and Sapko 2009).

Parameter settings

The wall material of the tunnel was concrete. Table 1 lists the thermal properties of the wall and the initial environment. The instantaneous ignition source was located 4.6 m from the head of the C tunnel. The wall was a rigid no-slip boundary, and numerical simulations were performed using heat transfer mechanisms and adiabatic boundaries.

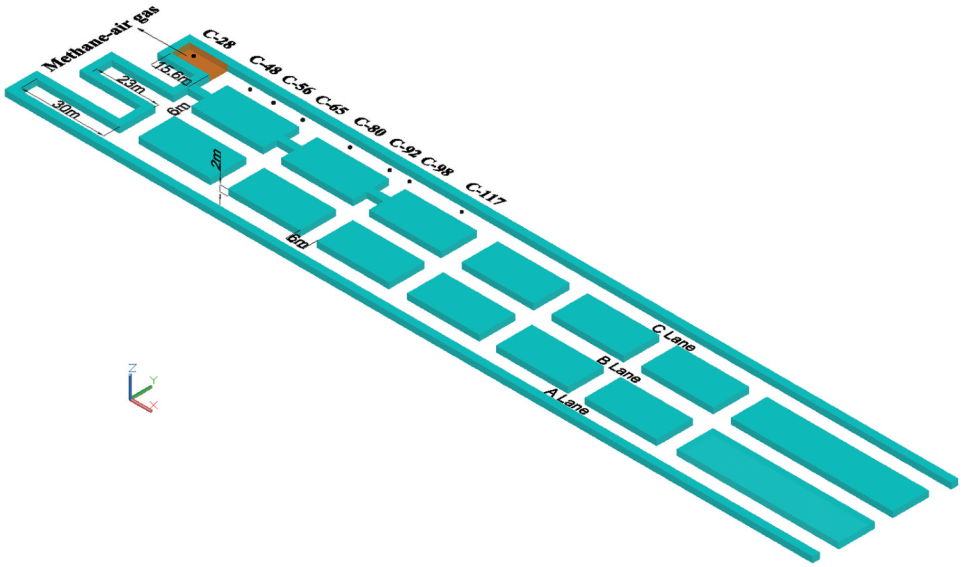

Figure 1. Geometric model of the Lake Lynn Experimental Mine.

Table 1. Parameter set for wall thermal performance and initial environment.

Items	Value
Density	1500 kg/m^3
Specific heat capacity	920 J/(kg·K)
Thermal conductivity	0.6 W/(m·K)
Emissivity	0.94
Temperature	300 K
Air pressure	101300 Pa
Gravity constant	9.8 m/s^2
Volume of mixed gas	187.2 m^3

Meshing and mesh independence testing

Mesh independence tests were performed with guaranteed computational accuracy to determine a reasonable mesh density. The experimental mine model was divided into two grid densities, and the results are shown in Figure 2. The results indicate that a high grid density of 0.1 m × 0.1 m × 0.1 m is not significantly better than a 0.2 m × 0.2 m × 0.2 m grid for characterization of the overpressure in the tunnel. Therefore, in this study, a 0.2 m × 0.2 m × 0.2 m grid was used in the numerical simulations to improve the computational efficiency. The computational domain was divided into 810, 172, and 10 in the x, y, and z directions, respectively, for a total of 1,393,200 grids.

Analysis of results and discussion

Analysis of the accuracy of the numerical simulation results

Figures 3 and 4 depict the decay curve of the peak overpressure along the alleyway and the curves of overpressure versus time at four monitoring points. The results of the adiabatic and heat transfer simulations were close to the measured values in terms of the peak pressure and shockwave attenuation trends. As shown in Figure 3, the farther the distance of the monitoring points, the smaller the error between the numerical simulation results and the measured values. The numerical simulation assumes that there are no obstacles in the tunnel, and the propagation of overpressure in unobstructed

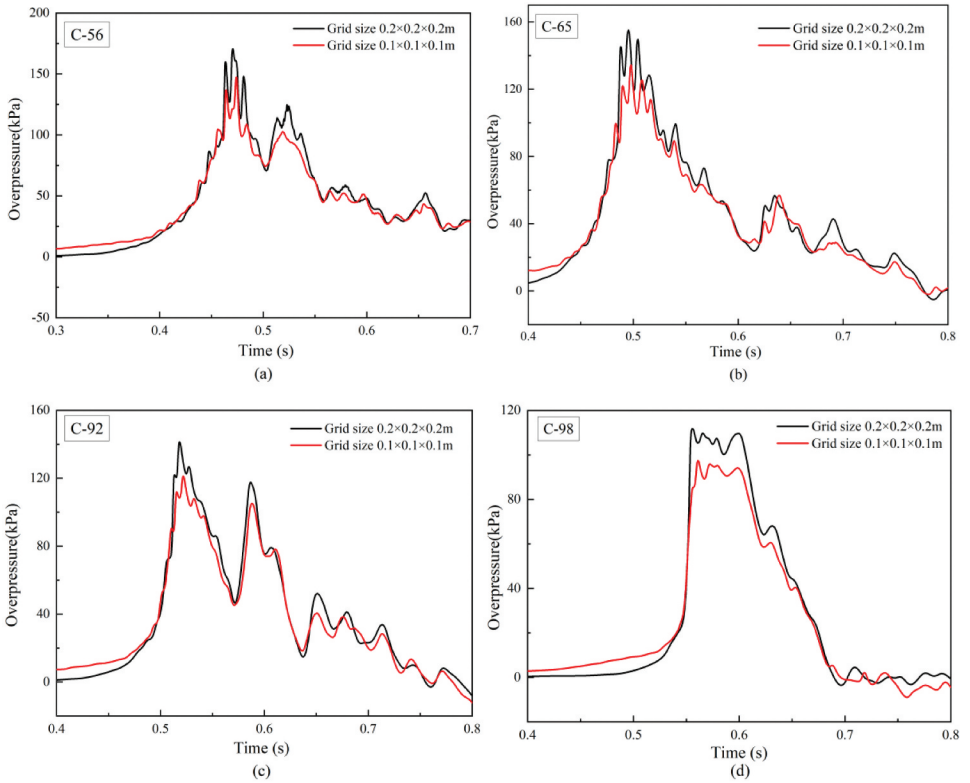

Figure 2. Mesh independence tests at monitoring sites.

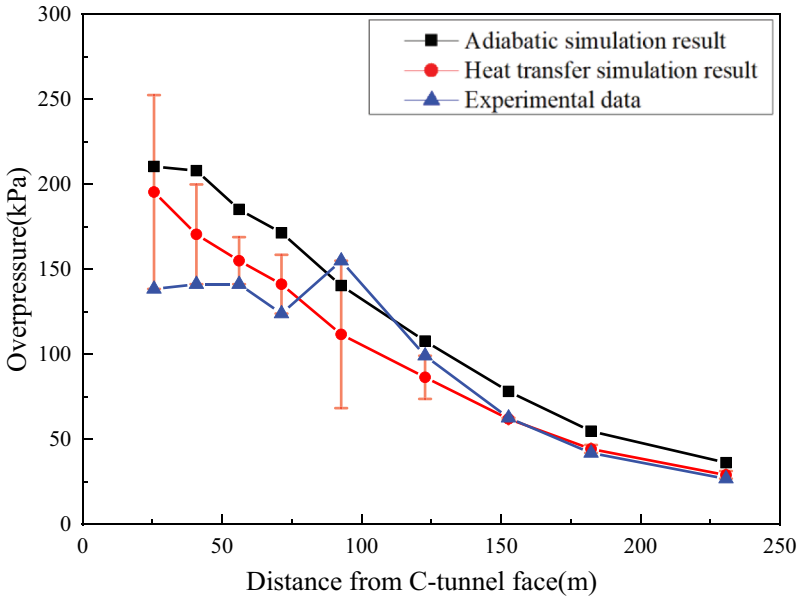

Figure 3. Attenuation variation curve of the peak overpressure in the tunnel.

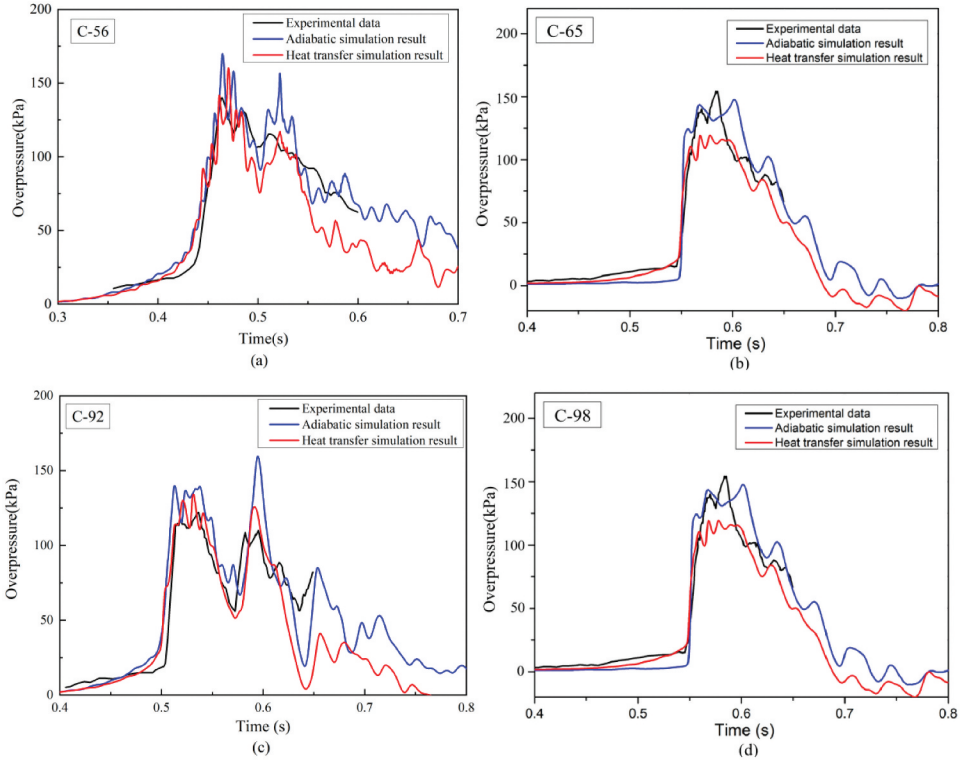

Figure 4. Comparison of measured and calculated values of overpressure at monitoring points.

tunnels should show a gradual decay trend (Chen et al. 2023; Zhang et al. 2016). However, in actual tunnels, there may be local obstacles, such as wood, cribs, etc., and the literature (Cashdollar, Urosek, and Sapko 2009) does not specify the location of obstacles, resulting in higher local pressure peaks at monitoring points C65 and C98 in the experimental values. A comparison of the calculated and experimental values revealed that the average errors for the heat transfer and adiabatic simulations were 5.18 and 10.67%, respectively. The oscillating overpressure change reflects the change laws of the flow field in a methane explosion space. Figure 4 shows that the overpressure oscillation change at the monitoring point calculated using GASFLOW-MPI was close to the experimental results. Therefore, the numerical analysis algorithm was effective, and the simulation results can be used to further analyze the variation laws of the velocity, temperature, and concentration fields in the explosion environment.

Analysis of shock wave overpressure in the tunnel

Based on simulations on the adiabatic and heat transfer, the overpressure curve of the shockwave versus time at different locations under adiabatic and nonadiabatic simulations was plotted to examine the propagation laws of shock waves in the tunnel. Figure 5 shows that the trends of the overpressure – time curves in the adiabatic and heat transfer simulations were similar; the overall trend exhibited a rapid increase and then a decrease. The peak overpressure decreased with increasing distance from the explosion source, and the peak overpressure was greater in the adiabatic simulations than in the heat transfer ones. As shown in Figures 5(a–d), the overpressure at the various monitoring sites after the methane explosion exhibited oscillatory characteristics, which are caused primarily by the "expansion – compression" of the high-temperature gas mixture. Figure 6(a) shows that in the C tunnel, at 0.52 s, the high-temperature gas from the methane explosion expanded dramatically, thereby forming

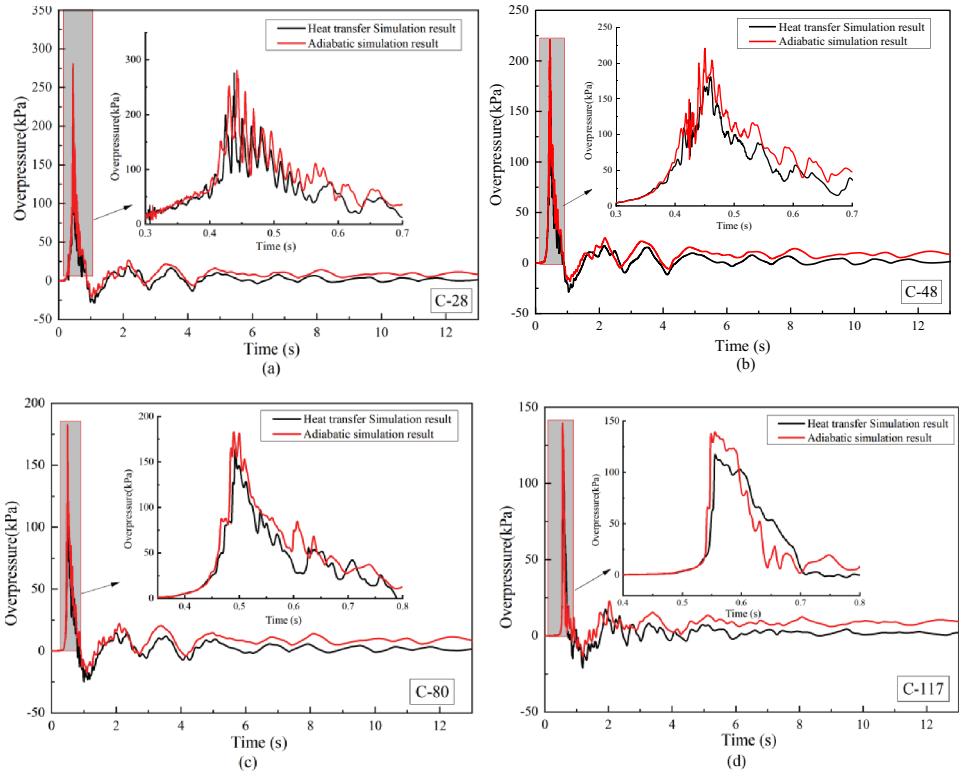

Figure 5. Curves of overpressure variation over time at monitoring points.

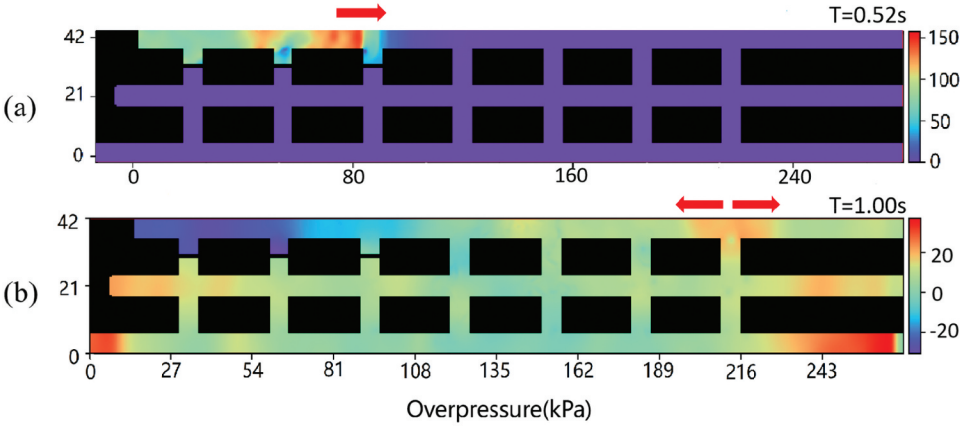

Figure 6. Overpressure distribution in heat transfer simulations in the tunnel (z = 1 m).

a high-pressure shockwave, which spread the air along the tunnel. Owing to the inertial effect of the outward movement of the high-temperature gas, the explosive combustion products continued to move forward, thus resulting in excessive expansion and negative pressure in the methane explosion reaction zone. As shown in Figure 6(b), the high-temperature gas began to migrate to the explosion reaction zone in response to negative pressure, thus resulting in gas compression in the explosion reaction zone. After several "expansion – compression" cycles of the high-temperature gas, the pressure in the tunnel returned to normal.

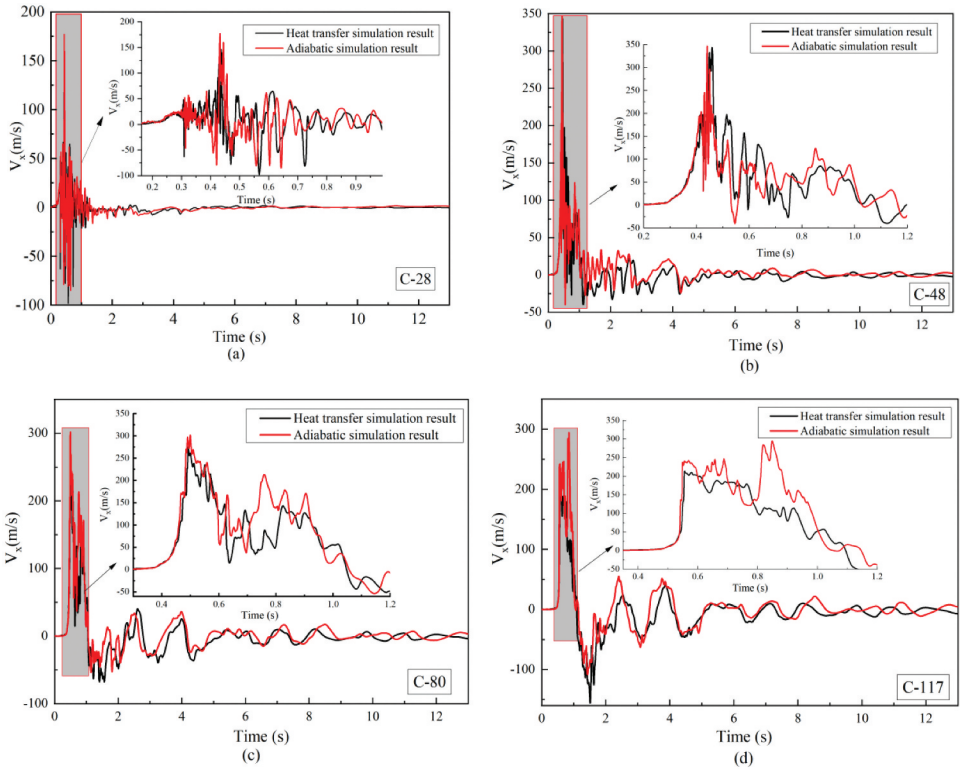

Figure 7. Curves of flow velocity variation over time at monitoring points.

Flow speed analysis in the tunnel

Figure 7 shows a plot of flow velocity versus time at four measurement points, which was used to analyze the gas flow in the adiabatic and heat transfer simulations. The oscillation amplitude of the flow speed profile decreased significantly with increasing distance from the ignition source. This was owing to the decrease in the amplitude of the overpressure oscillation, which resulted in a significant decrease in the oscillation amplitude of the flow speed. A comparison of Figure 7 reveals that the curve oscillation frequency and amplitude are higher in Figure 7(a) owing to the close proximity of the C-28 measurement point and the ignition source. During the propagation of the explosion shock wave, which is restricted by the alleyway, the shock wave was reflected and superimposed to form an overpressure oscillation, as shown in Figure 5(a). This resulted in a volatile C-28 flow field with considerable uncertainty, as shown in Figure 7(a). Therefore, the subsequent analysis did not consider the flow speed change law of the C-28 measurement point. The times at which the overpressure and flow speed each reach their peak and trough values were compared to investigate the relationship between flow speed and overpressure in the heat transfer simulation. Evidently, the time of peak flow speed lagged approximately 1 ms behind the time of peak overpressure, and the time of trough flow speed lagged 88.9, 408.0, and 328.4 ms, with an increase in distance exhibiting an increasing trend. Furthermore, as shown in Figure 6(a), the peak forward flow speed gradually decreased with increasing distance. The differential pressure between the peak overpressure in Figure 5 and the preceding tunnel overpressure caused the change in the forward flow speed. The differential pressure increased with distance from the ignition source, thus resulting in a decrease in the forward flow speed. In addition, a comparison of the adiabatic and heat transfer simulation curves in Figure 7 reveals that the adiabatic simulation had a higher positive peak flow velocity and a lower peak reverse flow velocity. This is because the overpressure peak was higher in the adiabatic simulation than in the heat transfer

simulation (see Figure 5) and the overpressure trough was the reverse. According to the energy equation (7) proposed by (Lin, Congguang, and Hui 2009), it can be observed that when the heat release rate is the same, the increase in heat loss leads to a decrease in the energy conversion of methane explosion into shock wave pressure and kinetic energy. Therefore, the peak and amplitude of the velocity curve in the heat transfer simulation are smaller than those under adiabatic simulation conditions.

$$q \quad q_1 + q_2 + W + F_K + L \tag{7}$$

Where q_1 and q_2 are the heat dissipation of high-temperature combustion products to the pipeline and unburned gas, kJ/kg; W is the added energy of shock wave, kJ/kg; F_K is the increase of kinetic energy of combustion products, kJ/kg; L is energy loss, kJ/kg.

Analysis of the temperature field in the tunnel

The temperature profiles of different monitoring points in the adiabatic and heat transfer simulations were plotted to analyze the temperature variation patterns of methane explosions in full-scale tunnels. Figure 8 shows that the temperature curves all exhibited a trend of rapid increase followed by a gradual decrease. This is because full-scale tunnels have ample space, thus allowing high-temperature gas to diffuse continuously toward the front of the tunnels. This results in a slight decrease in the temperature curve and a larger decrease in the temperature curve of the heat transfer simulation. Evidently from Figures 8(a–d), the adiabatic simulation of the peak temperature was greater than the heat transfer simulation of the peak temperature, and this phenomenon became more evident as the distance to the source increased. The peak temperature of the adiabatic simulation was approximately

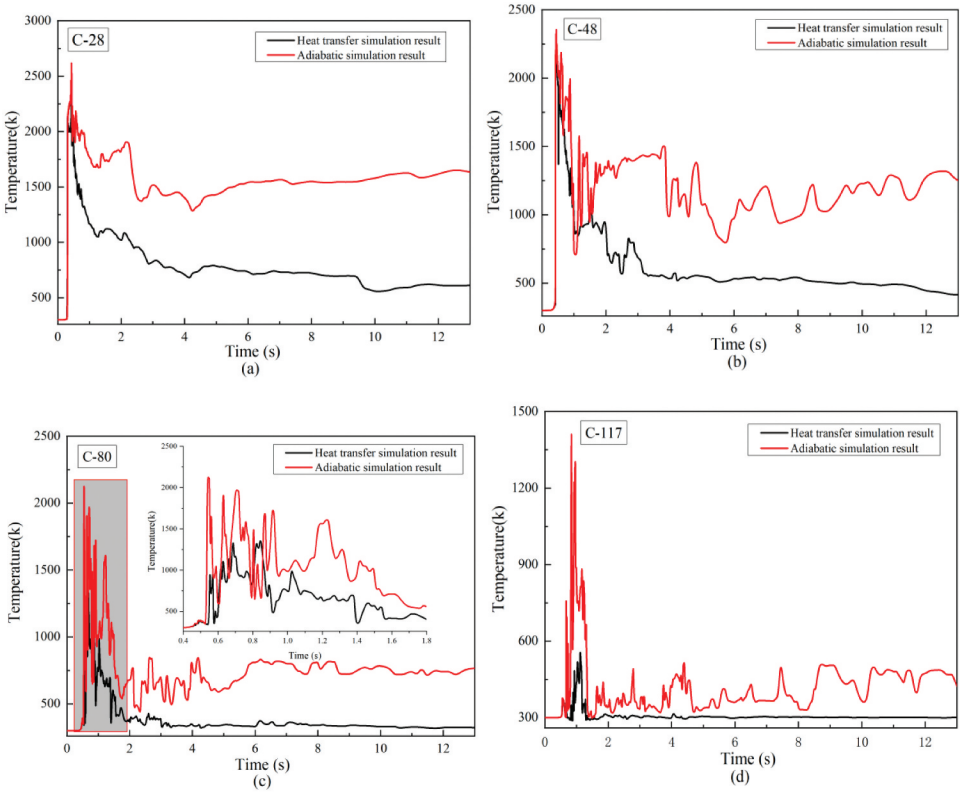

Figure 8. Curves of temperature variation over time at monitoring points.

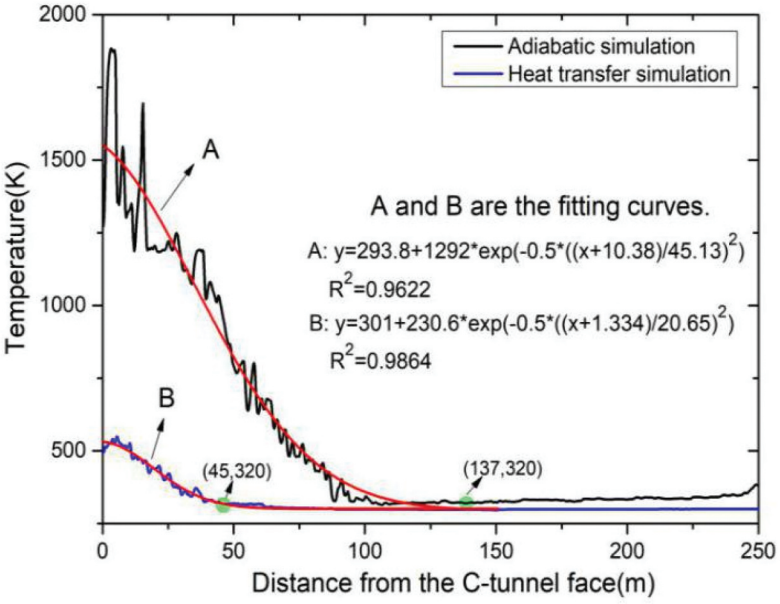

Figure 9. Temperature distribution curve in the tunnel at 13 s.

2.6 times that of the heat transfer simulation in C-117. The primary cause for this is that when the high-temperature gas diffuses forward, the exposed area of the tunnel wall increases, and greater convective heat loss occurs, thus increasing the temperature difference between the two simulations as the distance to the source of the explosion increases. According to Eq. (5), The primary cause for this is that when the high-temperature gas diffuses forward, the exposed area of the tunnel wall increases, and greater convective heat loss occurs, thus increasing the temperature difference between the two simulations as the distance to the source of the explosion increases.

The temperature in the tunnel was varied with distance at 13 s (see Figure 9) to investigate the temperature distribution law in the tunnel. Evidently, both the heat transfer and adiabatic simulations exhibited a linear decay in the temperature distribution pattern within the tunnel. At 13 s, the adiabatic simulated temperature field affected a distance of 137 m (approximately nine times the length of the gas accumulation in the tunnel before the methane explosion), whereas the heat transfer simulated temperature field only affected 45 m (approximately three times the length of the gas accumulation in the tunnel before the methane explosion). The temperature at both points was 320 K, and heat loss was the reason for the difference in the influence range between the two. Figure 10 shows the heat production and release curves of the methane explosions in a full-scale tunnel. With Stage I being the methane explosion reaction stage, the heat release and heat loss gradually increased, and the heat release reached a maximum at 0.9699 s when the heat loss was 159.3 MJ. With Stage II demonstrating the change in heat after the methane explosion reaction, the heat release did not change significantly. Moreover, the heat loss continued to increase, with 63.39% of the heat consumed in the form of heat loss at 13 s. Therefore, heat loss significantly affects the pattern of temperature change at individual monitoring points and the temperature distribution pattern within the tunnel following methane explosions.

Concentration field distribution of combustion products in the tunnel

The distribution pattern of combustion products of the explosion in a full-scale tunnel was analyzed using cloud plots of CO_2 concentration distribution at different moments in adiabatic and heat

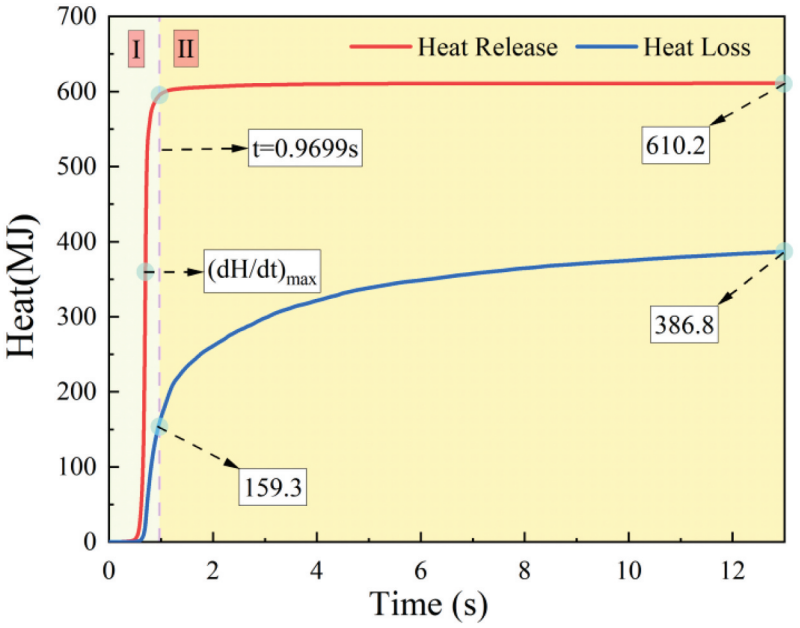

Figure 10. Total heat production and total heat release curves.

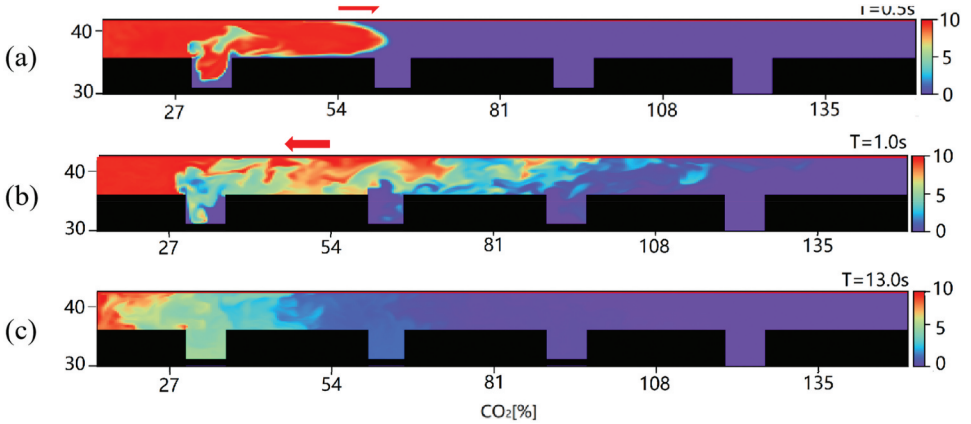

Figure 11. CO_2 concentration distribution in heat transfer simulation in the tunnel (z = 1 m).

transfer simulations (Figures 11 and 12). The figures show that CO_2 was not well mixed following methane explosions. Figures 11(a) and 12a show the CO_2 concentration distribution at 0.5 s. At this time, the CO_2 concentration distribution in the tunnel was concentrated, and CO_2 was transported forward at a positive flow velocity caused by the explosion shockwave. Figures 11(b) and 12b show the CO_2 concentration distribution at 1.0 s. Analysis in conjunction with Figures 6 and 7 indicates that negative pressure emerged in the methane explosion area at this time, and the combustion products of the explosion compressed toward the explosion area along with the reverse wind. Figures 11(c) and 12 (c) show the CO_2 concentration distribution at 13.0 s. As shown in Figure 5, the distribution of the explosive gas products in the flow field stabilized as the oscillation of the overpressure diminished. A comparison of Figures 13 and 14 revealed that the volume of CO_2 under adiabatic conditions was always larger than that in the heat transfer simulation during the same moment. According to the ideal gas law, PV = nRT, the gas expansion rate is proportional to the rate of temperature change. The

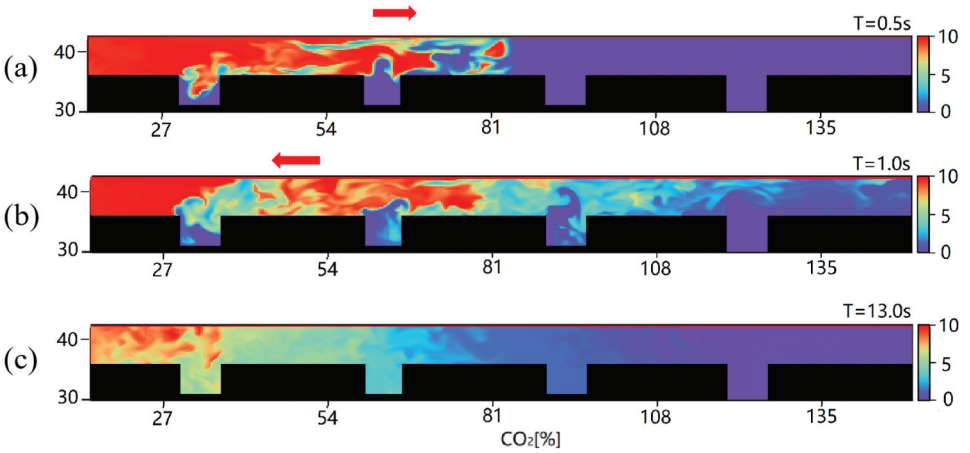

Figure 12. CO_2 concentration distribution in adiabatic simulation in the tunnel (z = 1 m).

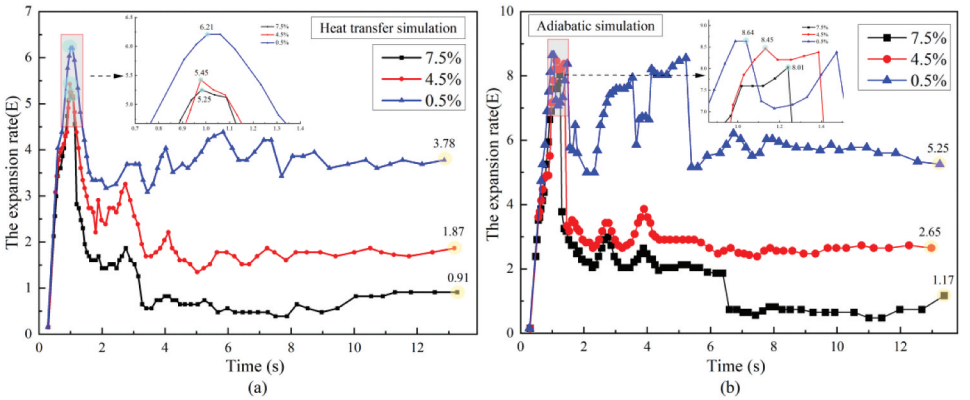

Figure 13. Curves of volumetric expansion ratio variation over time.

temperatures in the adiabatic simulation were significantly higher than those in the heat transfer simulation (Figure 8), thus generating a larger volume of gaseous product diffusion in the adiabatic simulation.

High-temperature gas flows back and forth with the shock wave in a tunnel during a methane explosion, thus causing dynamic changes in the expansion rate of the combustion products of the explosion. Based on the numerical simulation results of heat transfer and adiabatic conditions, the expansion coefficients for gas explosion were calculated using the formula Eq.. 8 (Lautkaski 1997) for different concentrations of CO_2. Dynamic curves of the volumetric expansion ratio at the center of Lane C were plotted with CO_2 concentrations of 0.5%, 4.5%, and 7.5% to understand the dynamic migration law of combustion products (CO_2) in the tunnel. Figure 13 shows that the expansion ratios of CO_2 under various concentrations of isosurfaces were different. However, they all exhibited a similar trend: beginning with a rapid increase, then oscillating and fluctuating, and finally stabilizing. Evidently from the expansion ratios of CO_2 concentrations of 0.5%, 4.5%, and 7.5% in the heat transfer simulation (Figure 13(a)), the maximum expansion ratios of the three CO_2 concentrations were 6.21, 5.45, and 5.25, whereas the final expansion ratios were 3.78,1.87, and 0.91, respectively. The higher the CO_2 concentration, the lower the calculated high-temperature gas expansion ratio. Figure 13(b) shows the ratio of volume expansion versus time in an adiabatic environment. A comparison of the results of the two simulations revealed that the volume expansion ratio for the same CO_2 concentration was

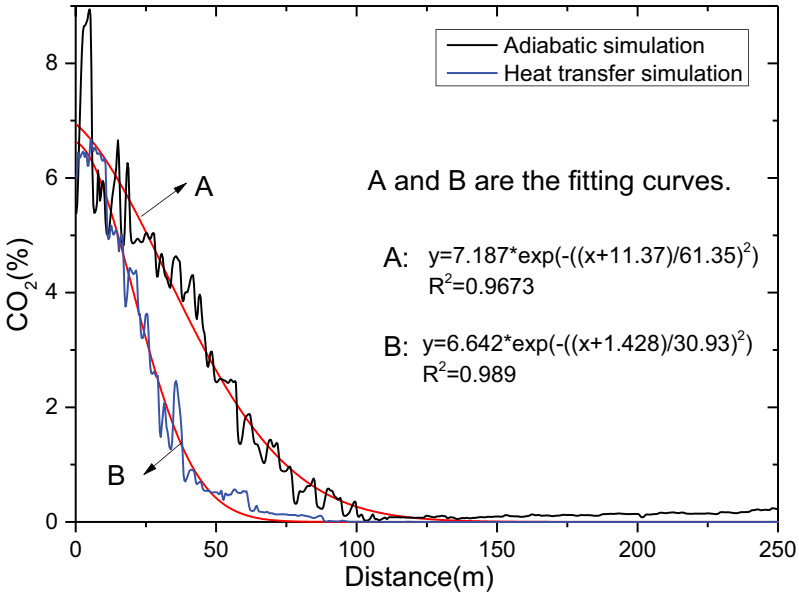

Figure 14. CO_2 concentration distribution curve in the tunnel at 13 s.

significantly higher in the adiabatic simulation than in the heat transfer simulation, in terms of both the maximum expansion ratio and final expansion ratio after stabilization. This is primarily owing to the absence of heat loss in the adiabatic environment and the higher temperatures of the gaseous products of the explosion in the tunnel, which have a more significant expansion effect.

$$\frac{V_f}{V_i} \quad \frac{N_f}{N_i}\frac{T_f}{T_i} \tag{8}$$

Where V_f is the expansion volume, m^3; V_i is the initial volume, m^3; N_f is the number of moles in the combustion products, mol; N_i is the number of moles in the unburned mixture, mol; T_f is flame temperature, K; T_i is the initial temperature, K.

Figure 14 depicts the CO_2 concentration distribution and the fitted curve at 13 s, which was used to analyze the concentration distribution of the combustion products of the explosion in the tunnel; curves A and B are the fitting curves of the distributions of CO_2 in the tunnel during the adiabatic and heat transfer simulations, respectively. The two fitting functions were Gaussian distribution functions. Figure 13 shows that following the stabilization of the flow field after the methane explosion, the CO_2 concentration was higher and the CO_2 concentration distribution area was farther away than it was in the heat transfer simulation. This is because of the larger volumetric gas expansion during the adiabatic simulation.

Conclusion

In this study, GASFLOW-MPI was used to study the dynamic distribution of the tunnel overpressure, flow velocity, temperature, and combustion products after a methane explosion in adiabatic and heat transfer simulations. The reliability of the numerical model was verified through a comparison with the results of LLEM experiments. However, due to the high cost and increased explosion risks associated with full-scale experiments, there are limited contents of full-scale experiments. In the future, more full-scale experiments will be conducted. The research findings can provide a theoretical basis for developing rescue plans for gas explosion accidents and reducing human casualties. The following conclusions were drawn.

(1) With the "expansion – compression" of high-temperature gas in the tunnel, the overpressure and flow speed exhibited similar oscillatory decay characteristics. As the distance from the explosion source increased, the oscillations in overpressure and flow speed gradually decreased in magnitude. However, a varying degree of lag was observed when the flow speed curve reached its peak or trough compared with the overpressure curve. Compared with the heat transfer simulation, the adiabatic simulation had a higher peak overpressure and lower trough overpressure, thus contributing to a higher positive peak flow speed and lower reverse peak flow speed.
(2) After the methane explosion, the temperature in the tunnel dropped rapidly, and the high-temperature gas volume expansion ratio changed dynamically. The maximum volumetric expansion of CO_2 reached 6.21, whereas the volumetric expansion after the stabilization of the flow field was 3.78. The temperature and gaseous product distributions along the alleyway tended to exhibit linear and Gaussian decay, respectively. Adiabatic simulations revealed higher CO_2 concentrations and a more distant distribution area within the tunnel compared with heat transfer simulations.
(3) In the numerical simulation of the methane explosion, the calculated peak pressure was approximately 15% higher when the heat transfer losses during the explosion were ignored. Further, the range of the gaseous product distribution and temperature fields in the tunnel was significantly larger, with a deviation of more than a factor of one between the two. In the full-scale experimental tunnel, when the flow field stabilized, the heat loss accounted for 63.01% of the total exothermic heat of the methane explosion.

Disclosure statement

The authors declare that they have no known competing financial interests or personal relationships that could have appeared to influence the work reported in this paper.

Funding

This work was supported by the Liaoning Provincial Natural Science Foundation funding program [grant numbers 2021-KF-23-05] and the basic scientific research business expenses of Central Universities [grant numbers 2022YQAQ09]. Baiwei Lei was also like to acknowledge China Scholarship Council for its financially supported.

Notes on contributors

Yuntao Liang graduated from Zhejiang University in 2010 with a Ph.D. degree. He primarily researches gas explosions, industrial combustible gas explosion safety, the theory and technology of coal mine fire prevention and control, the disaster-causing mechanism of thermo-dynamic compound hazards, and mine emergency rescue. He is currently the General Manager of China Coal Technology and Engineering Group Shenyang Research Institute Co., Ltd., Director of the State Key Laboratory of Coal Mine Safety Technology, a researcher, and a doctoral supervisor.

Baiwei Lei obtained his Ph.D. degree in 2015 from the China University of Mining and Technology (Beijing). His research mainly focuses on the mechanism of fire and explosion evolution, mine ventilation, and mine emergency rescue. He is currently an Associate Professor in the School of Emergency Management and Safety Engineering at China University of Mining and Technology (Beijing).

Shuanglin Song primarily researches coal mine fire monitoring and early warning technology, clean flame-retardant materials, and treatment techniques for hidden coal spontaneous combustion zones. He is currently the Deputy Director of the Experimental Center at China Coal Technology and Engineering Group Shenyang Research Institute Co., Ltd. State Key Laboratory of Coal Mine Safety Technology.

Jianjun Xiao obtained his Ph.D. degree from Tsinghua University and is primarily involved in scientific research on detonation, turbulent combustion, and multiphase flow. He is currently a Senior Researcher at the Institute of Thermal Technologies and Safety, Karlsruhe Institute of Technology in Germany.

Mike Kuznetsov received his Ph.D. degree from the Leningrad Institute of Technology and is primarily engaged in scientific research on detonation, turbulent combustion, and multiphase flow. He is currently a Senior Researcher at the Institute of Thermal Technologies and Safety, Karlsruhe Institute of Technology in Germany.

Thomas Jordan is currently conducting scientific research on detonation, turbulent combustion, and multiphase flow at the Institute of Thermal Technologies and Safety, Karlsruhe Institute of Technology in Germany.

Author Contributions

Formal analysis and resources L.Y.; writing – review and editing, L.B.; resources, S.S.; resources, X.J. formal analysis M. K.; writing – review T.J. All authors have read and agreed to the published version of the manuscript.

References

Ajrash, M. J., J. Zanganeh, and B. Moghtaderi. 2017. Deflagration of premixed methane–air in a large scale detonation tube. *Process Safety and Environmental Protection* 109:374–86. doi:10.1016/j.psep.2017.03.035.

Ajrash, M. J., J. Zanganeh, and B. Moghtaderi. 2018. Flame deflagration in side-on vented detonation tubes: A large scale study. *Journal of Hazardous Materials* 345:38–47. doi:10.1016/j.jhazmat.2017.11.014.

Cammarota, F., A. Di Benedetto, P. Russo, and E. Salzano. 2010. Experimental analysis of gas explosions at non-atmospheric initial conditions in cylindrical vessel. *Process Safety and Environmental Protection* 88 (5):341–49. doi:10.1016/j.psep.2010.05.001.

Cashdollar, K. L., J. E. Urosek, and M. J. Sapko. 2009. Results of in-mine research in support of the investigation of the sago mine explosion. *Centers for Disease Control and Preventi-On*.

Cheng, J., B. Zhang, H. D. Ng, Liu, H., and Wang, F . 2021. Effects of inert gas jet on the transition from deflagration to detonation in a stoichiometric methane-oxygen mixture. *Fuel* 285:119237. doi:10.1016/j.fuel.2020.119237.

Chen, D., C. Wu, J. Li, and K. Liao. 2023. An overpressure-time history model of methane-air explosion in tunnel-shape space. *Journal of Loss Prevention in the Process Industries* 82:105004. doi:10.1016/j.jlp.2023.105004.

Dahoe, A. E., and L. P. H. De Goey. 2003. On the determination of the laminar burning velocity from closed vessel gas explosions. *Journal of Loss Prevention in the Process Industries* 16 (6):457–78. doi:10.1016/S0950-4230(03)00073-1.

Davis, S. G., D. Engel, and K. Van Wingerden. 2014. Complex explosion development in mines: Case study-2010 upper big branch mine explosion. *Process Safety Progress* 34 (3):286–303. doi:10.1002/prs.11710.

Fernández-Tarrazo, E., A. L. Sánchez, A. Liñán, and F. A. Williams. 2006. A simple one-step chemistry model for partially premixed hydrocarbon combustion. *Combustion & Flame* 147:32–38. doi:10.1016/j.combustflame.2006.08.001.

Gao, K., S. Li, R. Han, R.-Z. Li, Z.-M. Liu, Z.-P. Qi, and Z.-Y. Liu. 2020. Study on the propagation law of gas explosion in the space based on the goaf characteristic of coal mine. *Safety Science* 127:104693. doi:10.1016/j.ssci.2020.104693.

Gieras, M., and R. Klemens. 2009. Experimental studies of explosions of methane-air mixtures in a constant volume chamber. *Combustion Science and Technology* 181 (4):641–53. doi:10.1080/00102200802665102.

Goldfarb, I., V. Gol'dshtein, G. Kuzmenko, and S. Sazhin. 1999. Thermal radiation effect on thermal explosion in gas containing fuel droplets. *Combustion Theory and Modelling* 3 (4):769–87. doi:10.1088/1364-7830/3/4/309.

Huang, J., X. Gao, and C. Wang. 2018. Flame acceleration and deflagration-to-detonation transition in narrow channels with thin obstacles. *Modern Physics Letters B* 32 (29):1850354. doi:10.1142/S0217984918503542.

Kundu, S., J. Zanganeh, and B. Moghtaderi. 2016. A review on understanding explosions from methane–air mixture. *Journal of Loss Prevention in the Process Industries* 40:507–23. doi:10.1016/j.jlp.2016.02.004.

Kuznetsov, M., G. Ciccarelli, S. Dorofeev, Alekseev, V., Yankin, Y., and Kim, T. H . 2002. DDT in methane-air mixtures. *Shock Waves*. 12(3):215–20. doi:10.1007/s00193-002-0155-0.

Kuznetsov, M., A. Denkevits, A. Veser, and A. Friedrich. 2022. Flame propagation regimes and critic-al conditions for flame acceleration and detonation transition for hydrogen-air mixtures at cryogenic temperatures. *International Journal of Hydrogen Energy* 47 (71):30743–56. doi:10.1016/j.ijhydene.2022.07.024.

Lautkaski, R. 1997. *Understanding vented gas explosions*. Finland: VTT Energy.

Lei, B., Q. Wei, R. Pang, and J. Xiao. 2023. The effect of hydrogen addition on methane/air explosion characteristics in a 20-L spherical device. *Fuel* 338:127351. doi:10.1016/j.fuel.2022.127351.

Lei, B. W., J. J. Xiao, M. Kuznetsov, and T. Jordan. 2022. Effects of heat transfer mechanism on methane-air mixture explosion in 20 L spherical device. *Journal of Loss Prevention in the Process Industries* 80:104864. doi:10.1016/j.jlp.2022.104864.

Li, Z., L. Chen, H. Yan, Fang, Q., Zhang, Y, Xiang, H., and Wang, S . 2021. Gas explosions of methane-air mixtures in a large-scale tube. *Fuel* 85:119239. doi:10.1016/j.fuel.2020.119239.

Lin, B., K. Congguang, and Z. Hui. 2009. Research on the influence of pipe wall heat dissipation on gas explosion propagation characteristics. *Journal of China University of Mining and Technology* 38 (1):1–4. doi:10.1016/j.applthermaleng.2017.02.084.
Luo, Z. M., and F. M. Cheng. 2013. Numerical simulation of gas explosion in confined space with FLACS. *Journal of the China Coal Society* 38:381–1387.
Lv, W., B. Liu, and L. Wang. 2013. Research on temperature changing law after coalmine explosion in roadway. *Journal of Harbin Institute of Technology* 45:108–13.
Mittal, M. 2017. Explosion pressure measurement of methane-air mixtures in different sizes of confinement. *Journal of Loss Prevention in the Process Industries* 46:200–08. doi:10.1016/j.jlp.2017.02.022.
Pang, L., Q. Zhang, T. Wang, D. C. Lin, and L. Cheng. 2012. Influence of laneway support spacing on methane/air explosion shock wave. *Safety Science* 50 (1):83–89. doi:10.1016/j.ssci.2011.07.005.
Qu, Z., X. Zhou, and H. Wang. 2008. Overpressure attenuation of shock wave during gas explosion. Journal of the China Coal Society 33:410–14.
Siegel, R., and J. R. Howell. 1992. *Thermal radiation heat transfer*. third ed. Washington: Hemisphere Publishing.
Tan, B., Y. Liu, H. Liu, H. Wang, and T. Li. 2021. Research on size effect of gas explosion in the Roadway. *Tunnelling and Underground Space Technology* 112:103921. doi:10.1016/j.tust.2021.103921.
Thomas, G. 2012. Some observations on the initiation and onset of detonation. *Physical and Engineering Sciences in Medicine* 370 (1960):715–39. doi:10.1098/rsta.2011.0368.
Travis, J. R., and D. P. Koch. 2014. GASFLOW simulations of a Bonfire test. *International Journal of Hydrogen Energy* 39 (24):13041–47. doi:10.1016/j.ijhydene.2014.06.026.
Valiev, D., V. Bychkov, V. Y. Akkerman, Law, C. K., and Eriksson, L. E. 2010. Flame acceleration in channels with obstacles in the deflagration-to-detonation transition. *Combustion & Flame* 157 (5):1012–21. doi:10.1016/j.combustflame.2009.12.021.
Vishwakarma, R. K., V. Ranjan, and J. Kumar. 2014. Comparison of explosion parameters for Methane–Air mixture in different cylindrical flameproof enclosures. *Journal of Loss Prevention in the Process Industries* 31:82–87. doi:10.1016/j.jlp.2014.07.002.
Wang, C., Y. Zhao, and E. K. Addai. 2017. Investigation on propagation mechanism of large scale mine gas explosions. *Journal of Loss Prevention in the Process Industries* 49:342–47. doi:10.1016/j.jlp.2017.07.011.
Xiao, J., W. Breitung, M. Kuznetsov, H. Zhang, J. R. Travis, R. Redlinger, and T. Jordan. 2017. GASFLOW-MPI: A new 3-D parallel all-speed CFD code for turbulent dispersion and combustion simulations Part II: First analysis of the hydrogen explosion in Fukushima Daiichi Unit 1. *International journal of hydrogen energy* 42 (12):8369–81. doi:10.1016/j.ijhydene.2017.01.219.
Xiao, J., M. Kuznetsov, and J. R. Travis. 2018. Experimental and numerical investigations of hydrogen jet fire in a vented compartment. *International Journal of Hydrogen Energy* 43 (21):10167–84. doi:10.1016/j.ijhydene.2018.03.178.
Xiao, H., and E. S. Oran. 2020. Flame acceleration and deflagration-to-detonation transition in hydrogen-air mixture in a channel with an array of obstacles of different shapes. *Combustion & Flame* 220:378–93. doi:10.1016/j.combustflame.2020.07.013.
Xiao, J., J. R. Travis, and M. Kuznetsov. 2015. Numerical investigations of heat losses to confinement structures from hydrogen-air turbulent flames in ENACCEF facility. *International Journal of Hydrogen Energy* 40 (38):13106–20. doi:10.1016/j.ijhydene.2015.07.090.
Ye, Q., G. G. X. Wang, Z. Jia, and C. Zheng. 2017. Experimental study on the influence of wall heat effect on gas explosion and its propagation. *Applied Thermal Engineering* 118:392–97. doi:10.1016/j.applthermaleng.2017.02.084.
Zhang, Q., and Q. J. Ma. 2015. Dynamic pressure induced by a methane–air explosion in a coal mine. *Process Safety & Environmental Protection* 93:233–39. doi:10.1016/j.psep.2014.05.005.
Zhang, Q., B. Qin, H. Yan, and D.-C. Lin. 2016. A methodology to predict shock overpressure decay in a tunnel produced by a premixed methane/air explosion. *Journal of Loss Prevention in the Process Industries* 44:275–81. doi:10.1016/j.jlp.2016.10.002.
Zhu, Y., D. Wang, Z. Shao, Xu, C., Li, M., and Zhang, Y . 2021. Characteristics of methane-air explosions in large-scale tunnels with different structures. *Tunn Undergr Space Technol* 109:103767. doi:10.1016/j.tust.2020.103767.
Zhu, Y., D. Wang, Z. Shao, X. Zhu, C. Xu, and Y. Zhang. 2020. Investigation on the overpressure of methane-air mixture gas explosions in straight large-scale tunnels. *Process Safety and Environmental Protection* 135:101–12. doi:10.1016/j.psep.2019.12.022.
Zipf, J. R. K., V. N. Gamezo, K. M. Mohamed, E. S. Oran, and D. A. Kessler. 2014. Deflagration-to-detonation transition in natural gas–air mixtures. *Combustion & Flame* 61 (8):2165–76. doi:10.1016/j.combustflame.2014.02.002.
Zipf, R. K., M. J. Sapko, J. F Brune, et al. 2007. Explosion pressure design criteria for new seals i-n U.S. coal mines. In *Deptartment of Health and Human Services, Centers for Disease Contr-ol and Prevention*, Vol. 76, 9500. Pittsburgh, PA: National Institute for Occupational Safety and Health, Pittsburgh Resea-rch Laboratory, IC.